



MOX-Report No. 20/2018

**A priori tests of a novel LES approach to compressible
variable density turbulence**

Bassi, C. ; Abbà, A.; Bonaventura L.; Valdetaro, L.

MOX, Dipartimento di Matematica
Politecnico di Milano, Via Bonardi 9 - 20133 Milano (Italy)

mox-dmat@polimi.it

<http://mox.polimi.it>

A priori tests of a novel LES approach to compressible variable density turbulence

Caterina Bassi⁽¹⁾

Antonella Abbà ⁽²⁾, Luca Bonaventura ⁽¹⁾, Lorenzo Valdetaro ⁽¹⁾

March 24, 2018

⁽¹⁾ MOX – Modelling and Scientific Computing,
Dipartimento di Matematica, Politecnico di Milano
Via Bonardi 9, 20133 Milano, Italy
`caterina.bassi@polimi.it`, `luca.bonaventura@polimi.it`,
`lorenzo.valdetaro@polimi.it`

⁽²⁾ Dipartimento di Scienze e Tecnologia Aerospaziali, Politecnico di Milano
Via La Masa 34, 20156 Milano, Italy
`antonella.abba@polimi.it`

Keywords: Large Eddy Simulation, compressible flows, variable density flows, density currents, Discontinuous Galerkin method

AMS Subject Classification: 65M60,65Z05,76F25,76F50,76F65

Abstract

We assess the viability of a recently proposed novel approach to LES for compressible variable density flows by means of *a priori* tests. The *a priori* tests have been carried out filtering a two-dimensional DNS database of the classic lock-exchange benchmark. The tests confirm that additional terms should be accounted for in subgrid scale modeling of variable density flows, with respect to the terms usually considered in the traditional approach. Several alternatives for the modeling of these terms are assessed and discussed.

1 Introduction

The limitations of the conventional approaches to Large Eddy Simulation (LES) of compressible, variable density flows have been recently discussed in [12], where the importance of additional contributions to the subgrid-scale terms in presence of strong density gradients is highlighted. Moreover, a first proposal for the modelization of these contributions is suggested. The purpose of the present work is to carefully assess the theoretical results in [12] by means of *a priori* tests. In particular, the relative importance of the different contributions to the subgrid scale stresses and the validity of the modeling proposals of [12] are evaluated.

The *a priori* tests have been carried out by filtering a two-dimensional Direct Numerical Simulation (DNS) database of the classic lock-exchange benchmark. We have chosen this test case because it has been widely investigated, both experimentally in [8], [15], [16], [22], [23] and numerically in [6], [7], [11], [14], [17], [18], [20], [19], [27]. This test case is also particularly appealing since it concerns complex flow evolution and turbulence phenomena, with breaking internal waves and Kelvin-Helmoltz instabilities, while being specified by simple initial and boundary conditions, see the discussion in [20]. Notice that we will focus here on the non-Boussinesq regime, which allows for strong density differences and which has not generally been addressed in the literature. Due to the transient character of the test-case, however, the statistical tools usually employed for the analysis of homogeneous or steady turbulent flows are not applicable in this context.

The numerical technique employed in the present investigation is a Discontinuous Galerkin (DG) discretization, see e.g. [5], [9], [10]. In particular, a modal DG discretization is employed, along the lines discussed in detail in [1], which has already been validated for lock-exchange simulations in [4]. This framework allows to compute in a straightforward way the filtered quantities as a projection onto a polynomial space of lower dimension with respect to the one employed for the DNS.

In this work, we show that some terms introduced in [12], which are usually neglected in the common density weighting approach to turbulence models for compressible turbulence, are not negligible. Furthermore, we show that the modeling proposal made in [12] is also partially in contrast with the *a priori* tests. Two alternative proposals for turbulence modeling in variable density compressible flows are then assessed in this work. The first approach is based on the modellization of the leading subgrid stress terms following

the eddy viscosity hypothesis. The *a priori* tests show low values for the correlations between the exact subgrid scale terms and the modeled ones, suggesting that the eddy viscosity approach may not be the best choice. If, despite the low correlations values, the eddy viscosity approach is preferred, the *a priori* tests results suggest the introduction of two different, dynamically computed eddy viscosities ν_1 and ν_ρ . The introduction of a scale similarity model for the leading subgrid stress terms considerably improves the results in terms of correlations. The correlations associated to the proposed similarity scale model are also higher than those associated to the traditional similarity scale approach for compressible flows.

The paper is organized as follows. Section 2 summarizes the results in [12]. Section 3 is devoted to the presentation of the *a priori* tests results. In section 4, alternative modeling approaches to those originally introduced in [12] are presented and assessed, while conclusions and perspectives for future developments are drawn in section 5.

2 Turbulence models for compressible variable density flows

This section summarizes the theoretical results presented in [12] on LES modeling for variable density, compressible flows. We start considering the incompressible Navier-Stokes equations. The usual approach to LES for incompressible flows consists in the application of a filter $\bar{\cdot}$ to the Navier-Stokes equations. When filtering the convective term in the momentum equation, this leads to the appearance of the following additional subgrid scale stress tensor:

$$\tau(u_i, u_j) = \overline{u_i u_j} - \bar{u}_i \bar{u}_j. \quad (1)$$

The most popular approach to model the subgrid stresses is based on the eddy viscosity concept and can be formulated as:

$$\tau(u_i, u_j) = -\nu_{\text{sgs}} \bar{\mathcal{S}}_{ij}, \quad (2)$$

where $\bar{\mathcal{S}}_{ij}$ are the components of the strain rate tensor of the resolved velocity field $\bar{\mathbf{u}}$ and the subgrid viscosity ν_{sgs} can be modeled, for example, using a Smagorinsky like model ([24], [13]).

The filtering of the compressible Navier-Stokes equations is more complex than that of the incompressible equations, since the advective term in the momentum equation is represented by a third order term $\rho u_i u_j$. Furthermore, a second order term ρu_i represents the

advective term of the continuity equation. In order to avoid the appearance of subgrid terms in the continuity equation, Favre filtering $\tilde{\cdot}$ is introduced as:

$$\tilde{f} = \frac{\overline{\rho f}}{\bar{\rho}}, \quad (3)$$

see e.g. the discussion in [21]. The expression for the subgrid stress tensor in the momentum equation is then:

$$\tau_{ij} = \bar{\rho}\theta(u_i, u_j) = \overline{\rho u_i u_j} - \bar{\rho}\tilde{u}_i\tilde{u}_j. \quad (4)$$

Notice that, while usually the isotropic and deviatoric parts of the subgrid stress are modeled separately, in this section the two terms are modeled together for the sake of simplicity. By analogy to what is done in equation (2) for incompressible flows, the common approach with density weighting to the modelization of τ_{ij} is given by:

$$\bar{\rho}\theta(u_i, u_j) = -\bar{\rho}\nu^{\text{sgs}}\tilde{\mathcal{S}}_{ij}^d. \quad (5)$$

Some theoretical arguments on the extension of relation (2) for incompressible flows to equation (5) for compressible flows can be found in [25] and [29]. The approach followed in [12] is instead quite different. The filtered values of $\overline{\rho u_i}$ and $\overline{\rho u_i u_j}$ are expressed as follows:

$$\overline{\rho u_i} = \bar{\rho}\tilde{u}_i = \bar{\rho}\bar{u}_i + \tau(\rho, u_i), \quad (6a)$$

$$\begin{aligned} \overline{\rho u_i u_j} &= \bar{\rho}\tilde{u}_i\tilde{u}_j + \bar{\rho}\theta(u_i, u_j) = \bar{\rho}\bar{u}_i\bar{u}_j + \bar{\rho}\tau(u_i, u_j) \\ &\quad + \bar{u}_i\tau(\rho, u_j) + \bar{u}_j\tau(\rho, u_i) + \tau(\rho, u_i, u_j), \end{aligned} \quad (6b)$$

where $\tau(\rho, u_i)$ and $\tau(\rho, u_i, u_j)$ are the generalized subgrid moments associated to the turbulent transport of density. Notice that, starting from equations (6), it is possible to derive basic relations between the standard filtered quantities and the Favre filtered ones as:

$$\tilde{u}_i = \bar{u}_i + \frac{\tau(\rho, u_i)}{\bar{\rho}}, \quad (7a)$$

$$\theta(u_i, u_j) = \tau(u_i, u_j) - \frac{\tau(\rho, u_i)\tau(\rho, u_j)}{\bar{\rho}^2} + \frac{\tau(\rho, u_i, u_j)}{\bar{\rho}}. \quad (7b)$$

As pointed out in [12], equations (7) are well established in the context of Reynolds and Favre averages; the introduction of the generalized central moments allows their extension to the case of a filter operator, which does not always satisfy the property $\overline{\tilde{f}} = \tilde{f}$. Notice that, if we substitute the expression of the Favre filtered

velocity in equation (7a) into the expression for the Favre filtered strain rate, we obtain:

$$\begin{aligned} \tilde{\mathcal{S}}_{ij} = \partial_j \tilde{u}_i + \partial_i \tilde{u}_j = \partial_j \bar{u}_i + \partial_i \bar{u}_j - \frac{\tau(\rho, u_i) \partial_j \bar{\rho} + \tau(\rho, u_j) \partial_i \bar{\rho}}{\bar{\rho}^2} \\ + \frac{\partial_j \tau(\rho, u_i) + \partial_i \tau(\rho, u_j)}{\bar{\rho}}. \end{aligned} \quad (8)$$

We can then rewrite $\bar{\mathcal{S}}_{ij}$ as follows:

$$\bar{\mathcal{S}}_{ij} = \tilde{\mathcal{S}}_{ij} + \frac{\tau(\rho, u_i) \partial_j \bar{\rho} + \tau(\rho, u_j) \partial_i \bar{\rho}}{\bar{\rho}^2} - \frac{\partial_j \tau(\rho, u_i) + \partial_i \tau(\rho, u_j)}{\bar{\rho}} \quad (9)$$

If now we substitute $\tau(u_i, u_j)$, modeled as in equation (2), in equation (7b) and we use equation (9), we have:

$$\begin{aligned} \theta(u_i, u_j) = & -\nu_{\text{sgs}} \left[\tilde{\mathcal{S}}_{ij} + \frac{\tau(\rho, u_i) \partial_j \bar{\rho} + \tau(\rho, u_j) \partial_i \bar{\rho}}{\bar{\rho}^2} \right. \\ & \left. - \frac{\partial_j \tau(\rho, u_i) + \partial_i \tau(\rho, u_j)}{\bar{\rho}} \right] \\ & - \frac{\tau(\rho, u_i) \tau(\rho, u_j)}{\bar{\rho}^2} + \frac{\tau(\rho, u_i, u_j)}{\bar{\rho}}. \end{aligned} \quad (10)$$

If we consider an eddy viscosity model also for the terms $\tau(\rho, u_i)$ and $\tau(\rho, u_i, u_j)$:

$$\tau(\rho, u_i) = -\nu_\rho \partial_i \bar{\rho}, \quad (11a)$$

$$\tau(\rho, u_i, u_j) = -\nu_{\rho u} (\partial_j \tau(\rho, u_i) + \partial_i \tau(\rho, u_j)), \quad (11b)$$

we can notice that the conventional hypothesis (5) is valid if the three eddy viscosities ν_{sgs} , ν_ρ and $\nu_{\rho u}$ satisfy the following hypothesis:

$$\nu_{\rho u} = \nu_{\text{sgs}}, \quad \nu_\rho = 2\nu_{\text{sgs}},$$

which are not generally valid.

In [12], an attempt is made to take into account some of the additional terms in equation (10). In particular, if equations (11b) together with equation (2) are assumed and the following hypothesis are considered

$$\nu_{\rho u} = \nu_{\text{sgs}}, \quad \nu_\rho \neq 2\nu_{\text{sgs}}, \quad (12)$$

$\theta(u_i, u_j)$ can be expressed as:

$$\theta(u_i, u_j) = -\nu_{\text{sgs}} (\partial_j \tilde{u}_i + \partial_i \tilde{u}_j) - \frac{\nu_\rho (\nu_\rho - 2\nu_{\text{sgs}})}{\bar{\rho}^2} \partial_i \bar{\rho} \partial_j \bar{\rho}. \quad (13)$$

The different terms of equations (7) and (10) will be carefully estimated by means of an *a priori* test, whose results are presented in the following section, in order to establish whether the hypothesis (12) can be actually considered valid.

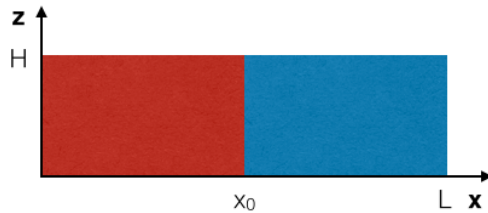


Figure 1: Initial datum for the lock-exchange configuration.

3 *A priori* tests results

The lock-exchange configuration employed in the *a priori* tests is represented in figure 1. In non dimensional units, the domain length is $L = 5$ and its height is $H = 1$, while the total duration of the simulation is $T = 25$. A membrane initially divides the rectangular container in two compartments (the position of the membrane is $x_0 = 2.5$ in the present computations). In our case, the two chambers are filled with the same fluid at different densities on the two sides of the membrane (higher density on the left and lower density on the right). Upon the removal of the membrane, the dense front moves rightward along the lower boundary, while the light front propagates leftward along the upper boundary. The ratio between the initial densities is $\gamma_r = 0.4$, the Mach number is $Ma = 0.1$, while the Reynolds number is equal to $Re = 2800$.

Notice that, as previously remarked, the model equations (compressible Navier-Stokes equations with gravity), their non dimensional formulation and the numerical discretization are the same as presented in [1] and [4], to which we refer for a complete description of the numerical method. Time integration has been performed with a five stages Strong Stability Preserving Runge-Kutta method described in [26].

Concerning the initial conditions, the initial density profile is given by:

$$\rho_0(x) = \frac{\gamma_r + 1}{2} - \frac{1 - \gamma_r}{2} \operatorname{erf} \left(\frac{x - x_0}{\sqrt{Re}} \right), \quad (14)$$

where x denotes the horizontal coordinate ([4], [6]). Since we are considering the compressible Navier-Stokes equations, it is necessary to specify the initial conditions also for pressure and temperature. The initial pressure distribution in the domain is computed assuming an hydrostatic pressure profile where the initial value at the top of the domain is imposed as in [4]. The initial datum for temperature is derived starting from density and pressure and using the

equation of state. Concerning the boundary conditions, the same slip boundary conditions as in [4] have been imposed.

For the space discretization, the polynomial degree $p = 7$ was employed, which entailed a number of degrees of freedom per element equal to $N_p = (p + 1)(p + 2)/2 = 36$. The choice of the polynomial degree and of the computational grid (composed approximately of 4000 elements) was made so as to obtain a total number of degrees of freedom similar to the one employed in [20] for two-dimensional Boussinesq simulations at the same Reynolds number. The mesh is built starting from a structured Cartesian mesh with $N_x = 104$, $N_z = 20$ quadrilaterals in the x, z directions. Each quadrilateral is then divided into $N_t = 2$ triangular elements. The mesh is uniform in all directions and the equivalent mesh spacing in each direction, taking into account the fact that high-order polynomials are employed, is given by:

$$\Delta_x = \frac{L}{N_x \sqrt{N_t N_p}}, \quad \Delta_z = \frac{H}{N_z \sqrt{N_t N_p}}, \quad (15)$$

where L and H are the length and height of the computational domain, respectively.

The grid filter and the test filter, necessary in order to carry out the *a priori* tests, are identified with the L_2 projection on the space of $\bar{p} = 4$ and $\hat{p} = 2$ piecewise polynomial functions, respectively. The grid filter scale can be computed, for the generic element K , as:

$$\Delta(K) = \frac{\bar{\Delta}_x \bar{\Delta}_z}{N_{\bar{p}}}, \quad (16)$$

with $\bar{\Delta}_x = \frac{L}{N_x \sqrt{N_t N_{\bar{p}}}}$ and $\bar{\Delta}_z = \frac{H}{N_z \sqrt{N_t N_{\bar{p}}}}$. The test filter scale is defined analogously, with the only difference that $N_{\bar{p}}$ is substituted by the number of degrees of freedom per element corresponding to the polynomial degree associated to the test filter.

The first quantity to be evaluated in the *a priori* tests is the difference, if any, between the filtered velocity and the Favre filtered velocity. The time evolution of the quantities

$$\max_{\Omega} \left(\frac{|\tilde{u}_i - \bar{u}_i|}{|\bar{u}_i|} \right), \quad i = 1, 2$$

is reported in figure 2. Here, Ω denotes the computational domain. We can notice that significant differences in the maximum values, up to 90%, are present.

Having verified that significant differences between the filtered velocity and the Favre filtered velocity can arise, we consider equa-

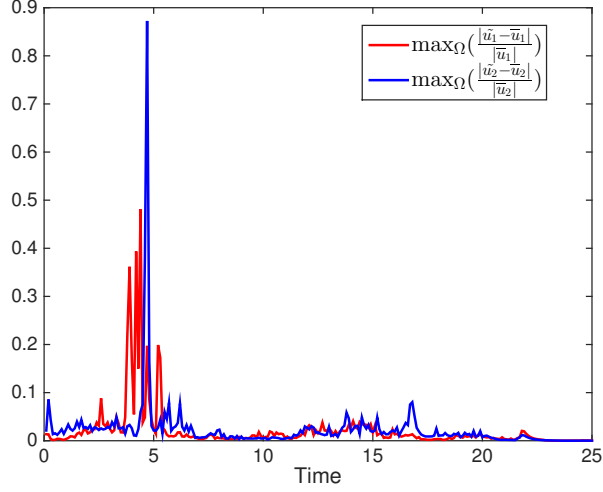


Figure 2: Maximum value over the domain Ω of the relative difference between the Favre filtered velocity and the filtered velocity, as a function of time.

tion (7b) and we rewrite the three contributions to $\theta(u_i, u_j)$ separately as:

$$\tau(u_i, u_j), \quad (17a)$$

$$b_{ij} = -\frac{\tau(\rho, u_i)\tau(\rho, u_j)}{\bar{\rho}^2}, \quad (17b)$$

$$c_{ij} = \frac{\tau(\rho, u_i, u_j)}{\bar{\rho}}. \quad (17c)$$

The time evolution of the Frobenius norm:

$$\|\theta\|_F = \sqrt{\int_{\Omega} \sum_{ij} \theta(u_i, u_j)^2 d\mathbf{x}} \quad (18)$$

for each of the three contributions (17) has been computed, together with the norm of $\theta(u_i, u_j)$ itself. Moreover, we have also considered the L_2 norm of the individual components of each tensor:

$$\|\theta(u_i, u_j)\|_{L_2} = \sqrt{\int_{\Omega} \theta(u_i, u_j)^2 d\mathbf{x}}, \quad \text{for } i, j = 1, \dots, d. \quad (19)$$

The time evolution of the maximum and minimum values

$$\max_{\Omega} \theta(u_i, u_j) \quad \min_{\Omega} \theta(u_i, u_j), \quad i, j = 1, \dots, d$$

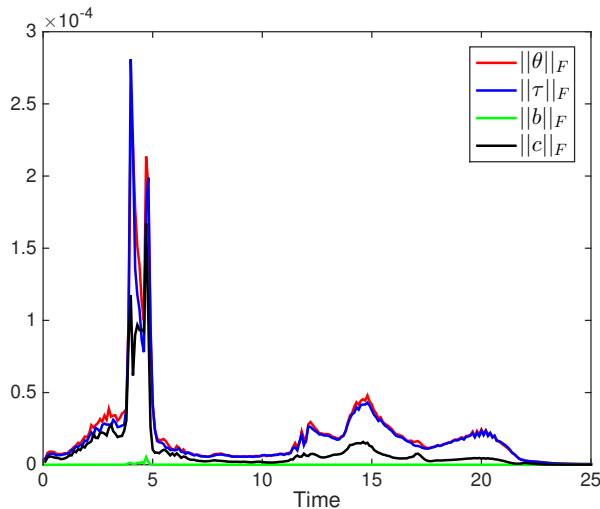


Figure 3: Frobenius norm of θ , τ , b and c as a function of time.

taken by the individual components of each tensor have also been evaluated. Analogous expressions have also been computed for $\tau(u_i, u_j)$, b_{ij} and c_{ij} .

In figure 3, the time evolution of the Frobenius norm (18) of θ , τ , b and c is shown. We can easily notice that the predominant contributions are those of θ and τ . Also the norm of c takes significant values, while the norm of b is 3 or 4 orders of magnitude smaller. If we look at figure 4, we can see that the L_2 norms of the single components of the different tensors (see equation (19)) confirm this trend. Moreover, we can also notice that the diagonal components are slightly larger than the off-diagonal ones.

The time evolution of the maximum (figure 5) and minimum values (figure 6) of the components of θ , τ , b and c is consistent with the previous results, confirming the predominance of τ and θ , followed by c , and the fact that b is far less important.

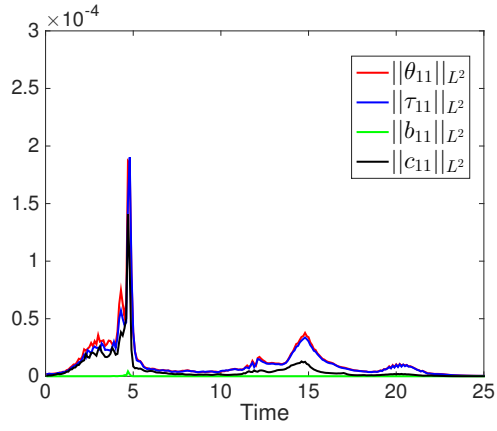
If we now compare equations (7b) and (10), we can see that $\tau(u_i, u_j)$ can be written as the sum of the following three contributions:

$$\tau_{ij}^{(1)} = -\tilde{S}_{ij}, \quad (20a)$$

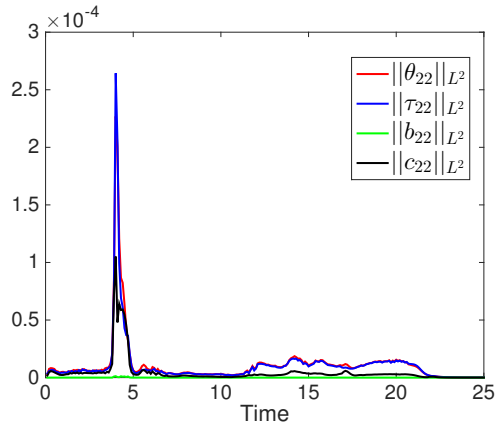
$$\tau_{ij}^{(2)} = -\frac{\tau(\rho, u_i)\partial_j\bar{\rho} + \tau(\rho, u_j)\partial_i\bar{\rho}}{\bar{\rho}^2}, \quad (20b)$$

$$\tau_{ij}^{(3)} = \frac{\partial_j\tau(\rho, u_i) + \partial_i\tau(\rho, u_j)}{\bar{\rho}}, \quad (20c)$$

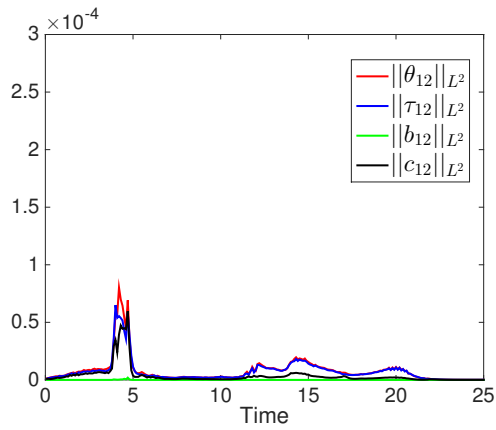
multiplied by ν_{sgs} . In figure 7, the Frobenius norm of the different



(a)

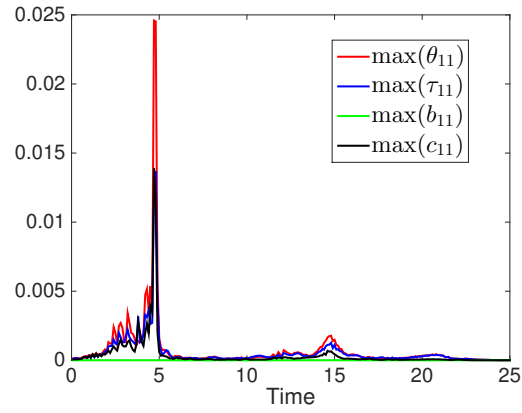


(b)

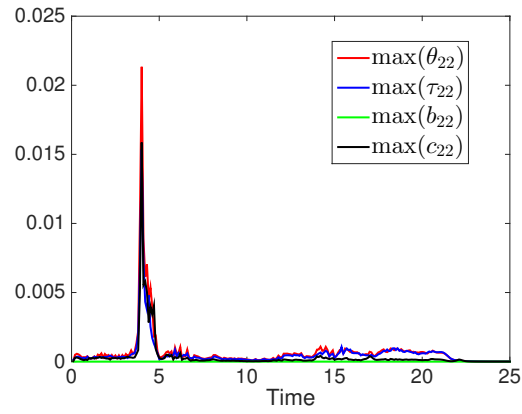


(c)

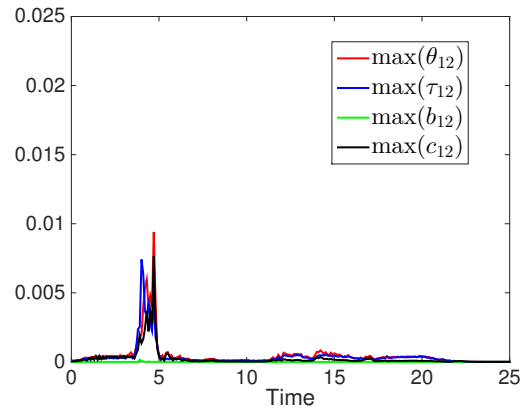
Figure 4: L_2 norm of the different components of θ , τ , b and c as a function of time. (a) First diagonal component. (b) Second diagonal component. (c) Off diagonal component.



(a)

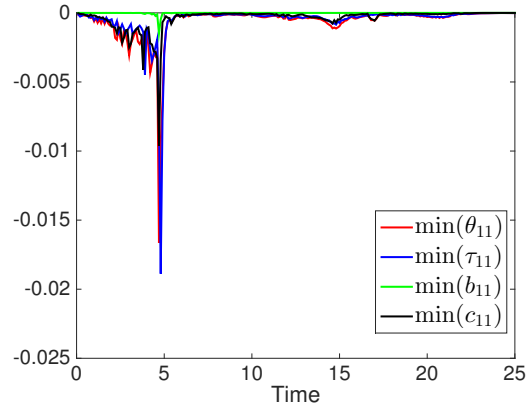


(b)

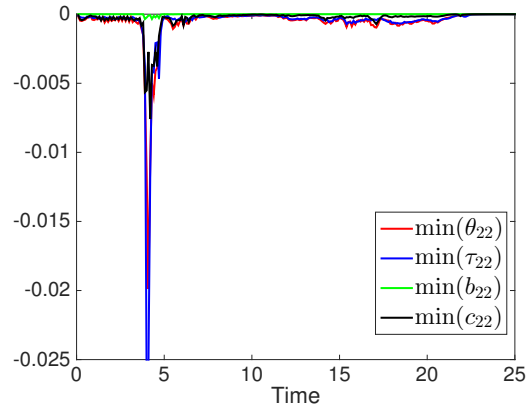


(c)

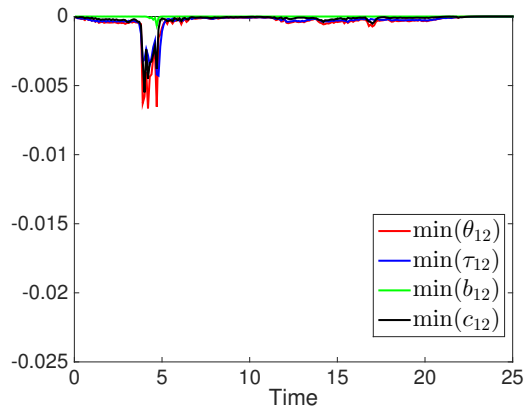
Figure 5: Maximum value over the domain Ω of the different components of θ , τ , b and c as a function of time. (a) First diagonal component. (b) Second diagonal component. (c) Off-diagonal component.



(a)



(b)



(c)

Figure 6: Minimum value over the domain Ω of the different components of θ , τ , b and c as a function of time. (a) First diagonal component. (b) Second diagonal component. (c) Off diagonal component.

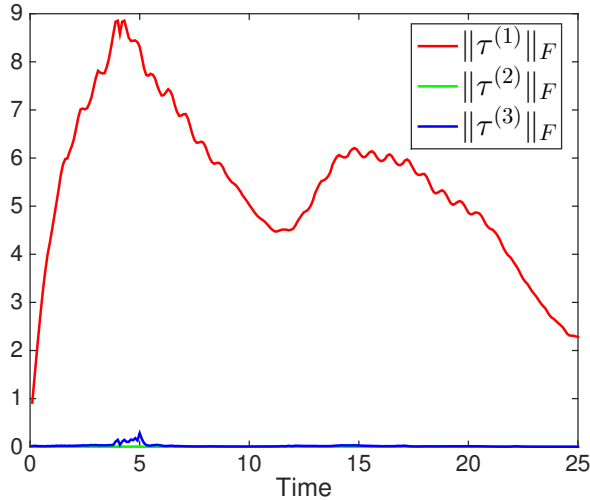


Figure 7: Frobenius norm of $\tau^{(1)}$, $\tau^{(2)}$ and $\tau^{(3)}$ as a function of time.

terms (20) is represented as a function of time. We notice that the contribution $\tau^{(1)}$ is much more important than the other two. A very similar trend is present in the L_2 norms of the different components of $\tau^{(1)}$, $\tau^{(2)}$ and $\tau^{(3)}$, see figure 8.

In figures 9 and 10, respectively, we show the time evolution of the maximum and minimum values over the domain Ω of $\tau^{(1)}$, $\tau^{(2)}$ and $\tau^{(3)}$. With respect to the evaluation in the Frobenius norm (see figure 7), we observe a more important contribution of $\tau^{(3)}$.

Concluding, if we consider equation (10), the terms which are not negligible are:

$$- \nu_{\text{sgs}} \tilde{S}_{ij}, \quad (21a)$$

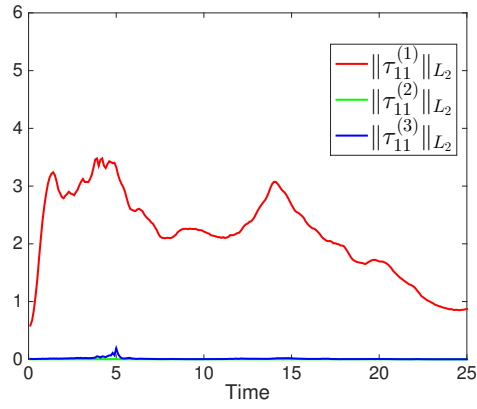
$$\nu_{\text{sgs}} \tau_{ij}^{(3)} = \nu_{\text{sgs}} \frac{\partial_j \tau(\rho, u_i) + \partial_i \tau(\rho, u_j)}{\bar{\rho}}, \quad (21b)$$

$$c_{ij} = \frac{\tau(\rho, u_i, u_j)}{\bar{\rho}}. \quad (21c)$$

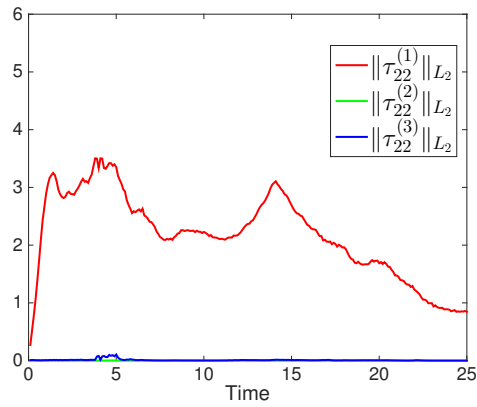
Notice that, in addition to the first term (21a), which is the only one usually considered in the traditional approach with density weighting for filtering in the compressible flows context, on the basis of the *a priori* tests, also the terms (21b) and (21c) have to be retained when strong density gradients are present.

This is in contrast with the modeling hypotheses proposed in [12], which are recalled here:

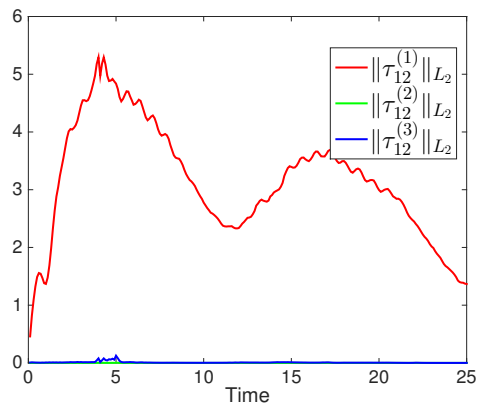
$$\nu_{\rho u} = \nu_{\text{sgs}}, \quad \nu_{\rho} \neq 2\nu_{\text{sgs}}. \quad (22)$$



(a)

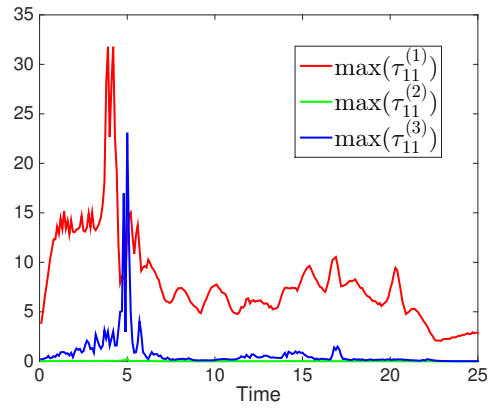


(b)

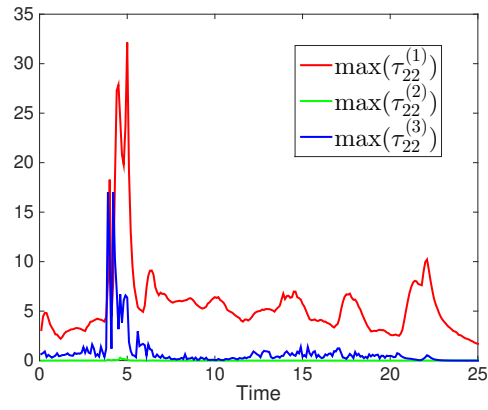


(c)

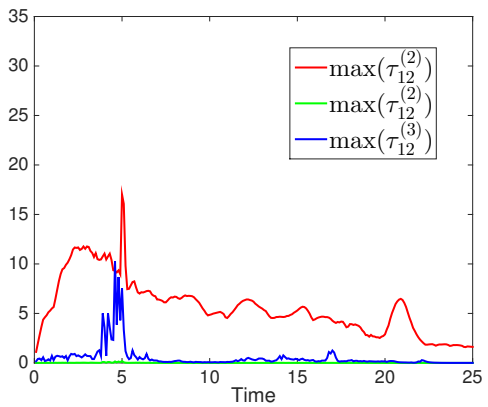
Figure 8: L^2 norm of the different components of $\tau^{(1)}$, $\tau^{(2)}$ and $\tau^{(3)}$ as a function of time. (a) First diagonal component. (b) Second diagonal component. (c) Off diagonal component.



(a)

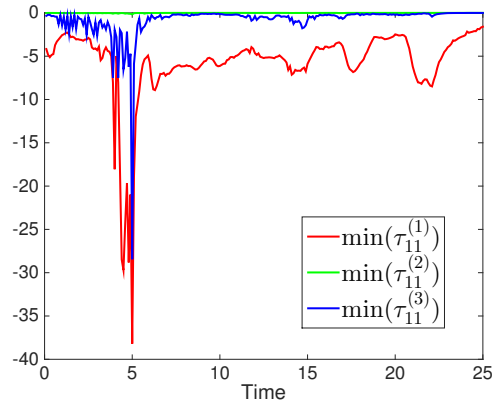


(b)

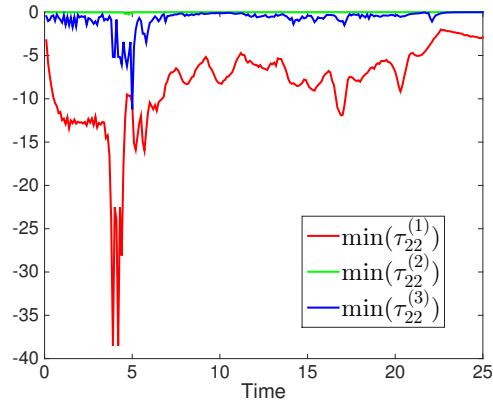


(c)

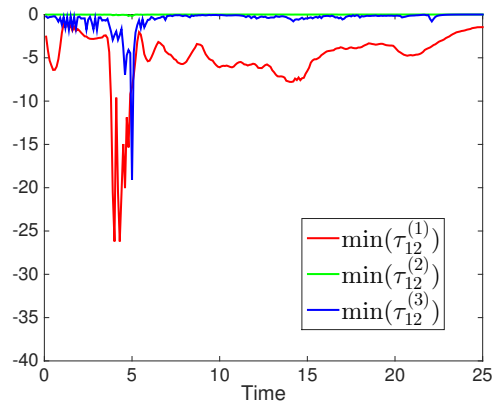
Figure 9: Maximum value over the domain Ω of $\tau^{(1)}$, $\tau^{(2)}$ and $\tau^{(3)}$ as a function of time. (a) First diagonal component. (b) Second diagonal component. (c) Off-diagonal component.



(a)



(b)



(c)

Figure 10: Minimum value over the domain Ω of $\tau^{(1)}$, $\tau^{(2)}$ and $\tau^{(3)}$ as a function of time. (a) First diagonal component. (b) Second diagonal component. (c) Off-diagonal component.

These hypotheses have the consequence that the terms $\nu_{\text{sgs}}\tau^{(3)}$ (see equation (21b)) and c_{ij} (equation (21c)), which are both non negligible according to the *a priori* tests, cancel each other. Notice also that the hypothesis (22) lead to the fact that the two terms $\nu_{\text{sgs}}\tau^{(2)}$ (equation (20b)) and b_{ij} (equation (17b)), which are negligible according to the *a priori* tests, are retained in the Germano formulation.

4 Alternative modeling hypothesis

In the previous section we have verified that, in addition to $-\nu_{\text{sgs}}\tilde{\mathcal{S}}_{ij}$, there are other important terms in the expression for the subgrid scale Favre stress, when dealing with flows characterized by strong density variations. However, we have also verified that some of the modeling hypotheses in [12] are not in good agreement with the previous results of the *a priori* tests. Another limitation of the approach in [12] is that a third order moment, which is difficult to model, is introduced in the expression for the subgrid scale Favre stress. As a consequence, we try to propose an alternative modeling hypothesis and to verify its validity by means of *a priori* tests.

Using the definition (3) of Favre average and substituting it in equation (6a), we rewrite equation (4) as:

$$\begin{aligned}
\overline{\rho\theta}(u_i, u_j) &= \overline{\rho u_i u_j} - \overline{\rho \tilde{u}_i \tilde{u}_j} & (23) \\
&= \frac{1}{2} [\overline{\rho u_i u_j} - \overline{\rho u_i \tilde{u}_j} + \overline{\rho u_i u_j} - \overline{\rho u_j \tilde{u}_i} \\
&\quad + \overline{\rho u_i \tilde{u}_j} - \overline{\rho \tilde{u}_i \tilde{u}_j} + \overline{\rho u_j \tilde{u}_i} - \overline{\rho \tilde{u}_j \tilde{u}_i}] \\
&= \frac{1}{2} [\tau(\rho u_i, u_j) + \tau(\rho u_j, u_i) - \overline{\rho \tilde{u}_i}(\tilde{u}_j - \bar{u}_j) - \overline{\rho \tilde{u}_j}(\tilde{u}_i - \bar{u}_i)] \\
&= \frac{1}{2} [\tau(\rho u_i, u_j) + \tau(\rho u_j, u_i) - \tilde{u}_i \tau(\rho, u_j) - \tilde{u}_j \tau(\rho, u_i)],
\end{aligned}$$

where $\tau(\rho u_i, u_j) = \overline{\rho u_i u_j} - \overline{\rho u_i} \bar{u}_j$ is the subgrid flux of ρu_i advected by u_j . As done in section (3) for the three contributions (17), we evaluate the time evolution of the Frobenius (figure 11) and the L^2 norms (figure 12) together with the time evolution of the maximum (figure 13) and minimum values (figure 14) of the terms $\tau(\rho u_i, u_j)$ and $-\tilde{u}_i \tau(\rho, u_j)$ appearing in equation (23). As it can be seen from figures 11 and 12, the contribution of $-\tilde{u}_i \tau(\rho, u_j)$, even if not negligible, is smaller than that of $\tau(\rho u_i, u_j)$. Figures 13 and 14, where the time evolution of the maximum and minimum values of $\tau(\rho u_i, u_j)$ and $-\tilde{u}_i \tau(\rho, u_j)$ over the whole domain is represented, further suggest that the term $-\tilde{u}_i \tau(\rho, u_j)$ should be retained, since it provides

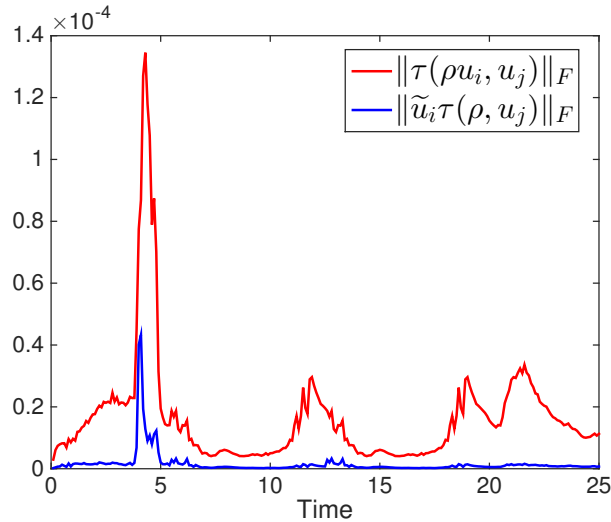


Figure 11: Frobenius norm of $\tau(\rho u_i, u_j)$ and $\tilde{u}_i \tau(\rho, u_j)$ as a function of time.

a contribution which is not completely negligible with respect to $\tau(\rho u_i, u_j)$.

We propose two different modeling approaches for the terms $\tau(\rho, u_i)$ and $\tau(\rho u_i, u_j)$. The first approach is of eddy viscosity type, while the second one extends the similarity scale hypothesis, firstly proposed in [3] and successively extended to compressible flows in [28], to compressible variable density flows. The two approaches are described in the following, together with the results of additional *a priori* tests performed to verify the validity of these new hypotheses.

4.1 Eddy viscosity approach

Considering an eddy viscosity approach, the two terms $\tau(\rho u_i, u_j)$ and $\tau(\rho, u_i)$ are modeled as:

$$\tau(\rho u_i, u_j) = -\nu_1 \partial_j \overline{\rho u_i} = -\nu_1 \partial_j (\overline{\rho} \tilde{u}_i), \quad (24a)$$

$$\tau(\rho, u_i) = -\nu_\rho \partial_i \overline{\rho}. \quad (24b)$$

As a first *a priori* test of this modelling assumption, we evaluate the correlations between $\tau(\rho u_i, u_j)$ and $\partial_j (\overline{\rho u_i})$ (see equation (24a)) and between $\tau(\rho, u_i)$ and $\partial_i \overline{\rho}$ (see equation (24b)), given respectively

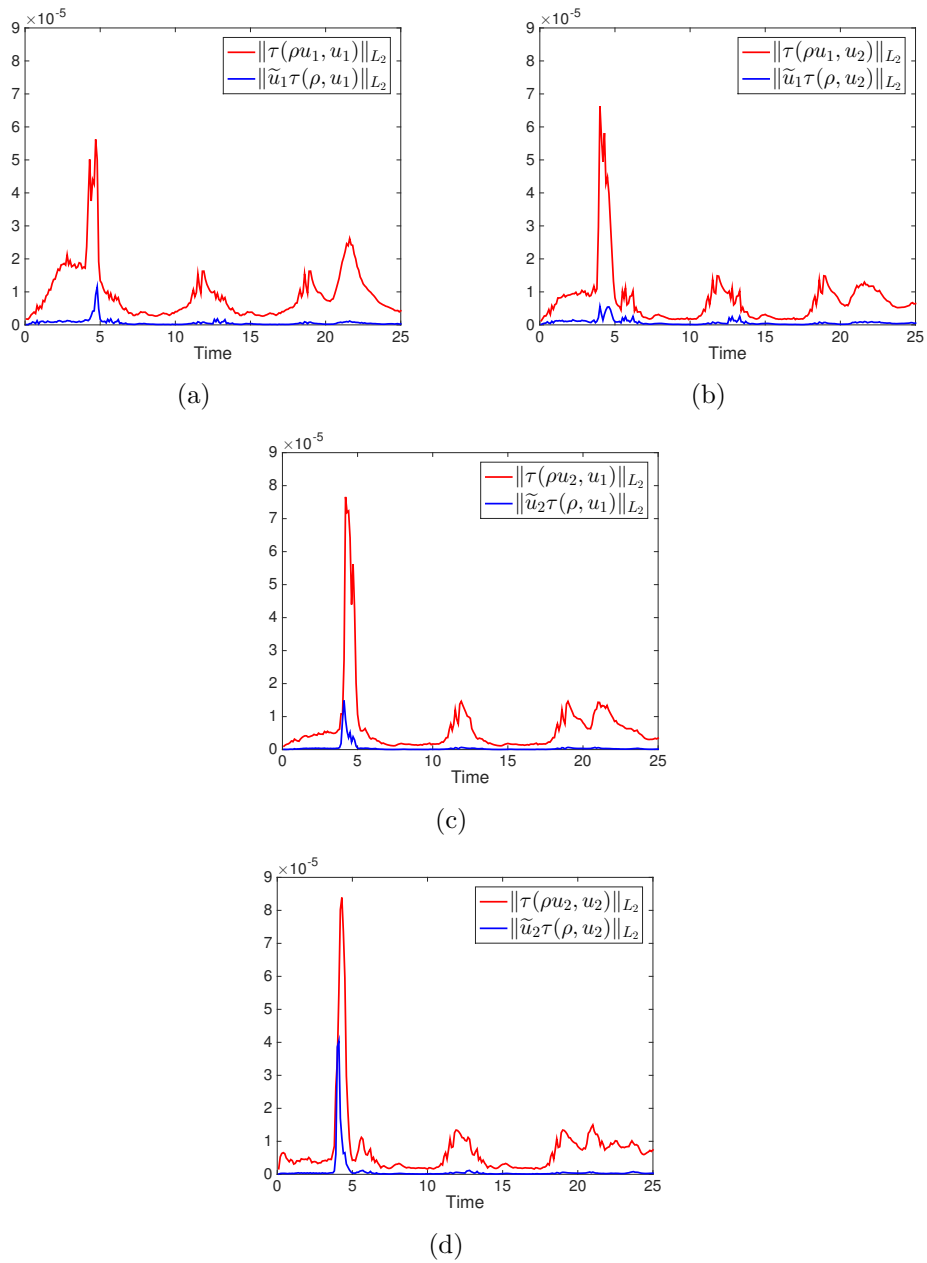


Figure 12: L^2 norm of $\tau(\rho u_i, u_j)$ and $\tilde{u}_i \tau(\rho, u_j)$ as a function of time. (a) Component 11. (b) Component 12. (c) Component 21. (d) Component 22.

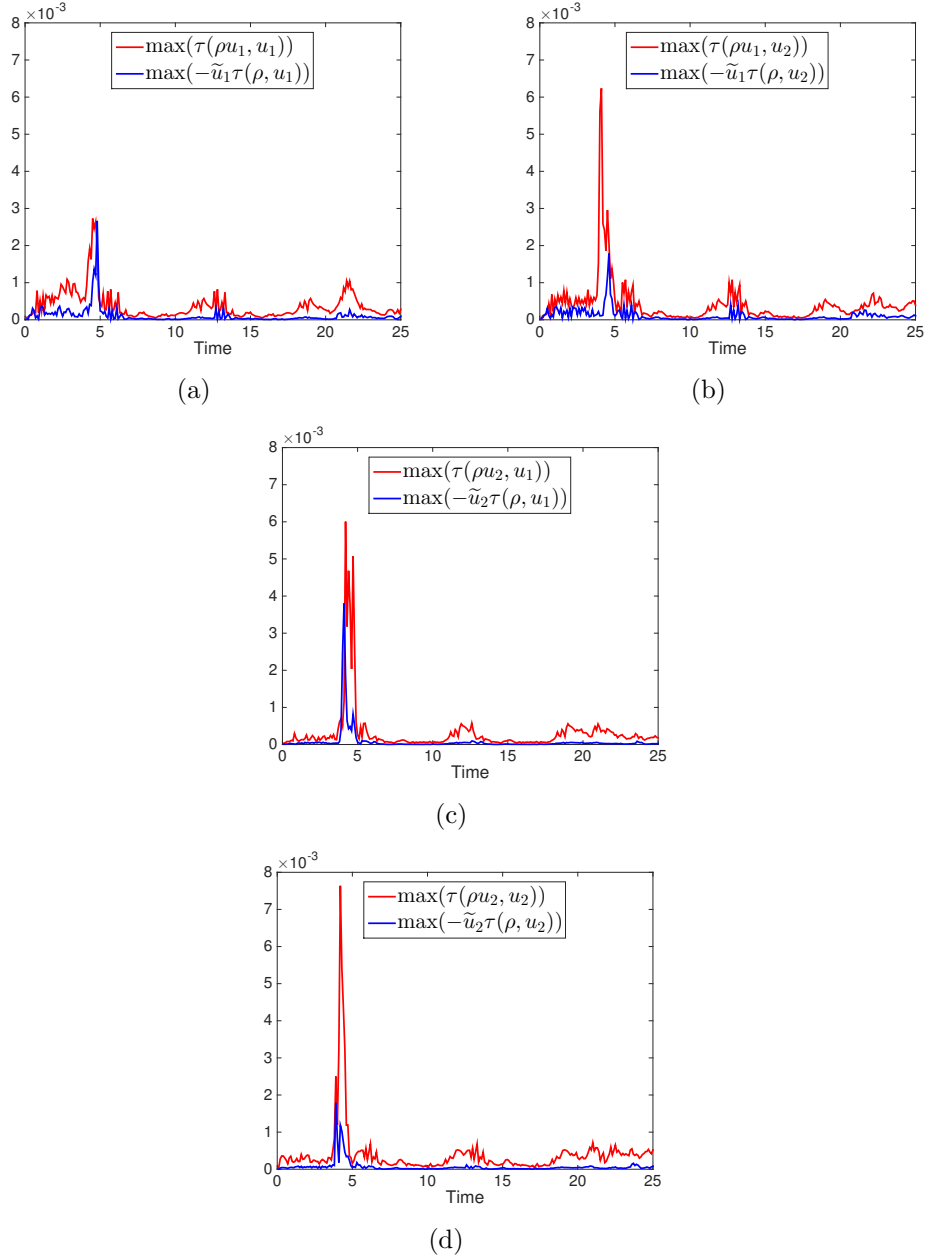
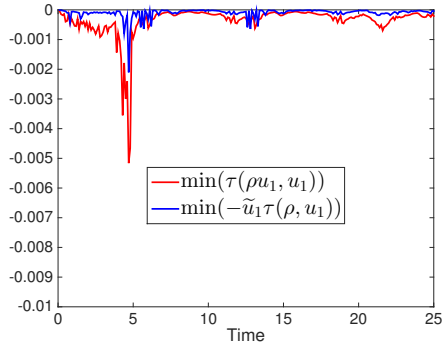
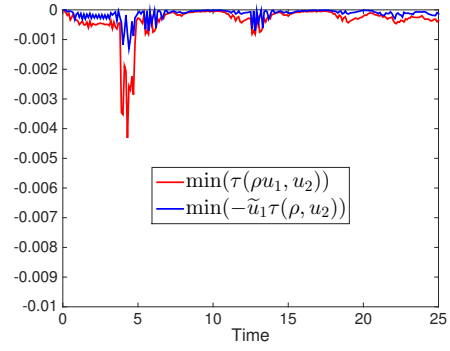


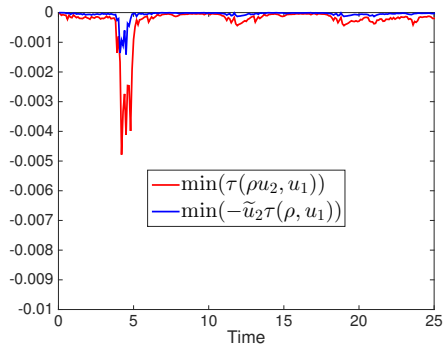
Figure 13: Maximum value over the domain Ω of $\tau(\rho u_i, u_j)$ and $\tilde{u}_i \tau(\rho, u_j)$ as a function of time. (a) Component 11. (b) Component 12. (c) Component 21. (d) Component 22.



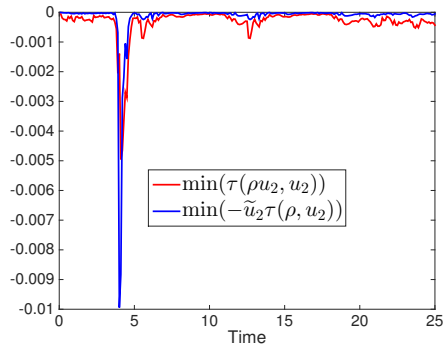
(a)



(b)



(c)



(d)

Figure 14: Minimum value over the domain Ω of $\tau(\rho u_i, u_j)$ and $\tilde{u}_i \tau(\rho, u_j)$ as a function of time. (a) Component 11. (b) Component 12. (c) Component 21. (d) Component 22.

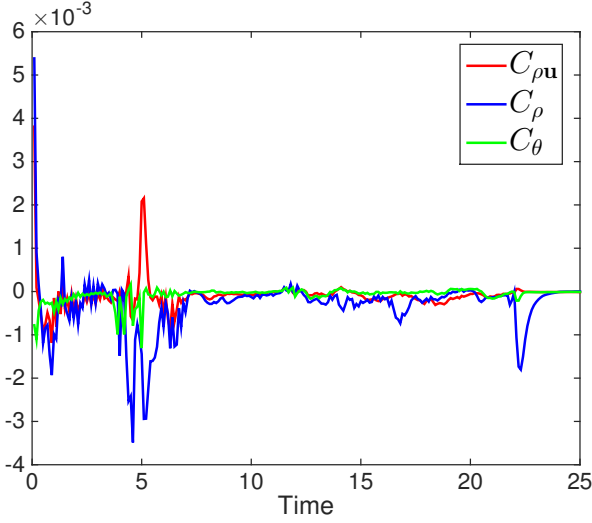


Figure 15: Correlations $C_{\rho\mathbf{u}}$, C_ρ and C_θ , corresponding to equations (25a), (25b) and (26), as a function of time.

by:

$$C_{\rho\mathbf{u}} = \frac{\frac{1}{|\Omega|} \int_{\Omega} \tau(\rho u_i, u_j) \partial_j \overline{\rho u_i} d\mathbf{x}}{\sqrt{\frac{1}{|\Omega|^2} \int_{\Omega} |\tau(\rho u_i, u_j)|^2 d\mathbf{x} \int_{\Omega} |\partial_j(\overline{\rho u_i})|^2 d\mathbf{x}}}, \quad (25a)$$

$$C_\rho = \frac{\frac{1}{|\Omega|} \int_{\Omega} \tau(\rho, u_i) \partial_i \overline{\rho} d\mathbf{x}}{\sqrt{\frac{1}{|\Omega|^2} \int_{\Omega} |\tau(\rho, u_i)|^2 d\mathbf{x} \int_{\Omega} |\partial_i \overline{\rho}|^2 d\mathbf{x}}}. \quad (25b)$$

In figure 15 these quantities are shown, together with the correlation between $\theta(u_i, u_j)$ and $\tilde{\mathcal{S}}_{ij}$ given by the following equation:

$$C_\theta = \frac{\frac{1}{|\Omega|} \int_{\Omega} \theta(u_i, u_j) \tilde{\mathcal{S}}_{ij} d\mathbf{x}}{\sqrt{\frac{1}{|\Omega|^2} \int_{\Omega} |\theta(u_i, u_j)|^2 d\mathbf{x} \int_{\Omega} |\tilde{\mathcal{S}}_{ij}|^2 d\mathbf{x}}}. \quad (26)$$

The quantities $\theta(u_i, u_j)$ and $\tilde{\mathcal{S}}_{ij}$ are those which are usually set proportional to each other in the conventional approach to turbulence modeling for compressible flows. Notice that the fact that mainly negative correlations arise is due to the fact that a minus sign is present on the right-hand side of equations (5), (24a) and (24b).

The correlation between $\theta(u_i, u_j)$ and $\tilde{\mathcal{S}}_{ij}$ is low in absolute value. Notice also that, even though the hypotheses (24a) and (24b) appear to improve the results with respect to the traditional hypothesis (this is true in particular for C_ρ), also $C_{\rho\mathbf{u}}$ and C_ρ remain low. On the other hand, low correlation values in *a priori* tests are somewhat

typical for eddy viscosity models, as discussed for example in [2] for the case of a turbulent channel flow benchmark.

In order to try to obtain a simpler approach with respect to that of equations (24) and since we can notice that both the subgrid fluxes in equations (24) are advected by the velocity field u_i , we verify by means of additional *a priori* tests if the simplification $\nu_1 = \nu_\rho$ can be introduced. Notice that the simplification $\nu_1 = \nu_\rho$ implicitly implies that we are considering scalar values for ν_1 and ν_ρ . As a preliminar remark notice however that, if we assume $\nu_1 = \nu_\rho$, we go back to the conventional model $\bar{\rho}\theta(u_i, u_j) = -\bar{\rho}\nu_1\tilde{\mathcal{S}}_{ij}$, where the only difference could be the introduction of an alternative expression for the eddy viscosity ν_1 with respect to the conventional $\nu_{\text{sgs}} = C_S\Delta^2|\tilde{\mathcal{S}}|$.

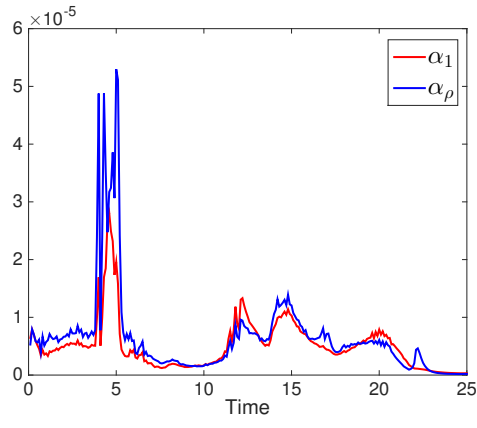
In order to simply compare the two quantities $\nu_{1,ij} = \frac{\tau(\rho u_i, u_j)}{\partial_j \bar{\rho} u_i}$ and $\nu_{\rho,i} = \frac{\tau(\rho, u_i)}{\partial_i \bar{\rho}}$, we compute the two following expressions:

$$\alpha_1 = \frac{\|\tau(\rho u_i, u_j)\|_F}{\|\partial_j \bar{\rho} u_i\|_F}, \quad \alpha_\rho = \frac{\|\tau(\rho, u_i)\|_F}{\|\partial_i \bar{\rho}\|_F}. \quad (27)$$

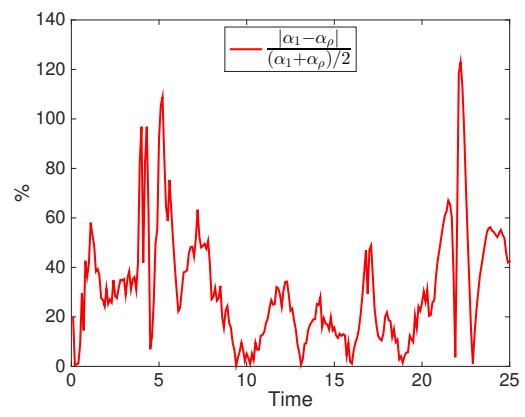
Notice that we compute separately the Frobenius norms of the numerator and of the denominator in the expressions of $\nu_{1,ij}$ and $\nu_{\rho,i}$, in order not to have problems with integration points in which the modeled terms at the denominator become zero. This implies that α_1 and α_ρ are just rough approximations of the size of ν_1 and ν_ρ .

In figure 16(a), we represent the time evolution of the two quantities in equations (27). We can notice that, even if the order of magnitude of the two quantities is the same, consistent differences between them are present. If we consider the time evolution of the relative difference between α_1 and α_ρ (figure 16(b)), we can see that relative differences up to 100% arise. As a consequence, even if the order of magnitude of ν_1 and ν_ρ appears to be the same, it is safer not to identify the two eddy viscosities in order not to risk to neglect additional terms, with respect to the traditional formulation, which can be important also when ν_1 and ν_ρ are slightly different between each other.

Concluding, if, despite the low correlations values, an eddy viscosity approach is preferred, the better way to implement it could be the introduction of a dynamic procedure for the determination of ν_1 and ν_ρ separately.



(a)



(b)

Figure 16: (a) Time evolution of the quantities α_1 and α_ρ . (b) Time evolution of the relative difference $\frac{|\alpha_1 - \alpha_\rho|}{(\alpha_1 + \alpha_\rho)/2}$ expressed in percentage.

4.2 Similarity scale approach

In the framework of a similarity scale approach, we propose instead the following models for the terms $\tau(\rho u_i, u_j)$ and $\tau(\rho, u_i)$:

$$\tau(\rho u_i, u_j) = c_1 \left(\overline{\rho u_i \widetilde{u}_j} - \overline{\rho u_i} \widetilde{u}_j \right), \quad (28a)$$

$$\tau(\rho, u_i) = c_\rho \left(\overline{\rho u_i} - \overline{\rho} \widetilde{u}_i \right), \quad (28b)$$

where it should be noticed that the second filtering operation is realized by means of the $\bar{\cdot}$ filter, rather than the Favre filter $\widetilde{\cdot}$, since, in this case, the unfiltered density would be necessary, which cannot be computed in a LES (see [28]). As in the eddy viscosity approach, the two constants c_1 and c_ρ can be determined employing a dynamic procedure.

Notice that our similarity scale approach is an extension to compressible variable density flows of the conventional similarity scale approach, first proposed in [3] and successively extended to compressible flows in [28]. The conventional similarity scale approach is given by:

$$\overline{\rho} \theta(u_i, u_j) = c \overline{\rho} \left(\overline{\widetilde{u}_i \widetilde{u}_j} - \widetilde{u}_i \widetilde{u}_j \right), \quad (29)$$

where a dynamic procedure can be employed for the determination of the constant c .

In order to see if the introduction of similarity scale models provides better results with respect to the eddy viscosity approach, we evaluate by means of the *a priori* tests the time evolution of the following correlations:

$$C_{\rho \mathbf{u}}^{sim} = \frac{\frac{1}{|\Omega|} \int_{\Omega} \tau(\rho u_i, u_j) \left(\overline{\rho u_i \widetilde{u}_j} - \overline{\rho u_i} \widetilde{u}_j \right) d\mathbf{x}}{\sqrt{\frac{1}{|\Omega|^2} \int_{\Omega} |\tau(\rho u_i, u_j)|^2 d\mathbf{x} \int_{\Omega} \left| \overline{\rho u_i \widetilde{u}_j} - \overline{\rho u_i} \widetilde{u}_j \right|^2 d\mathbf{x}}}, \quad (30a)$$

$$C_{\rho}^{sim} = \frac{\frac{1}{|\Omega|} \int_{\Omega} \tau(\rho, u_i) \left(\overline{\rho u_i} - \overline{\rho} \widetilde{u}_i \right) d\mathbf{x}}{\sqrt{\frac{1}{|\Omega|^2} \int_{\Omega} |\tau(\rho, u_i)|^2 d\mathbf{x} \int_{\Omega} \left| \overline{\rho u_i} - \overline{\rho} \widetilde{u}_i \right|^2 d\mathbf{x}}}. \quad (30b)$$

These correlations are analogous to those defined in equations (25) for the eddy viscosity case. In figure 17, the time evolution of the two correlations (30) is presented, together with the time evolution of the correlation C_{θ}^{sim} (associated to the conventional similarity scale model in equation (29)), which is computed as follows:

$$C_{\theta}^{sim} = \frac{\frac{1}{|\Omega|} \int_{\Omega} \overline{\rho} \theta(u_i, u_j) \overline{\rho} \left(\overline{\widetilde{u}_i \widetilde{u}_j} - \widetilde{u}_i \widetilde{u}_j \right) d\mathbf{x}}{\sqrt{\frac{1}{|\Omega|^2} \int_{\Omega} |\overline{\rho} \theta(u_i, u_j)|^2 d\mathbf{x} \int_{\Omega} \left| \overline{\rho} \left(\overline{\widetilde{u}_i \widetilde{u}_j} - \widetilde{u}_i \widetilde{u}_j \right) \right|^2 d\mathbf{x}}}. \quad (31)$$

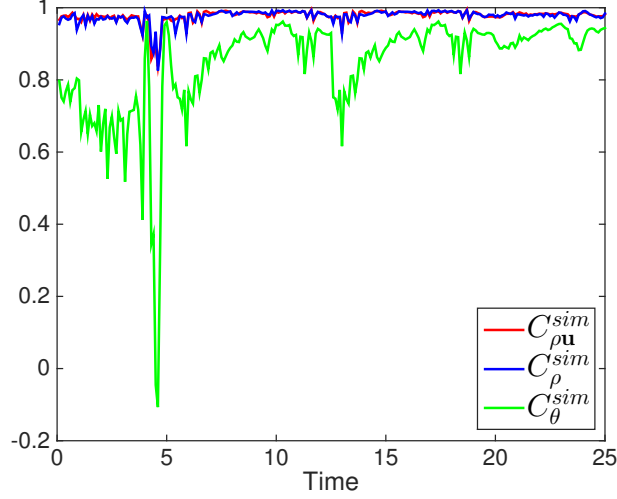


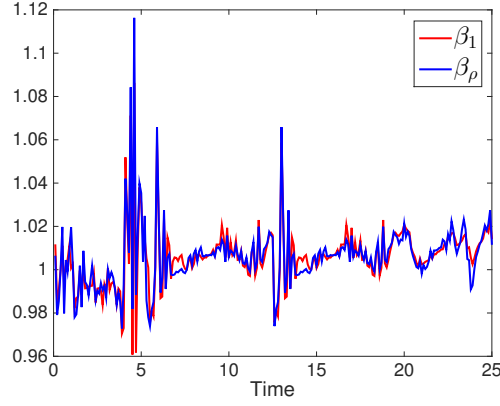
Figure 17: Correlations $C_{\rho\mathbf{u}}^{sim}$, C_{ρ}^{sim} (equations (30a) and (30b)) and correlation C_{θ}^{sim} (equation (31)), as a function of time.

We can notice that the correlation values $C_{\rho\mathbf{u}}^{sim}$ and C_{ρ}^{sim} (red and blue curves) are considerably higher with respect to the values of $C_{\rho\mathbf{u}}$ and C_{ρ} obtained with the eddy viscosity approach (see figure 15). Moreover, they are also higher with respect to C_{θ}^{sim} (green curve), associated to the traditional similarity scale approach. We can then conclude that a similarity scale approach as in equations (28), with the dynamic computation of the two constants c_1 and c_{ρ} , or even a mixed model (if too little dissipation is introduced by the scale similarity model alone), could be a better choice with respect to an eddy viscosity approach and also with respect to the traditional similarity scale model for compressible flows.

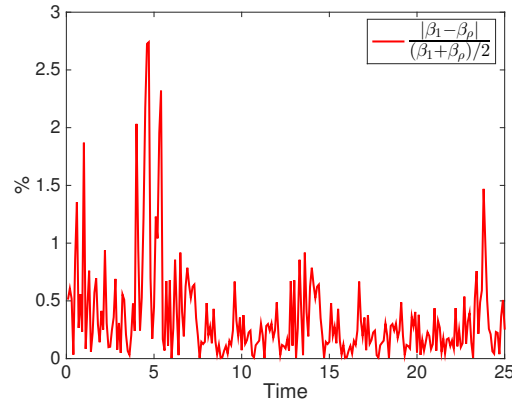
Analogously to what has been done for the eddy viscosity approach, we estimate the quantities c_1 and c_{ρ} , in order to have an idea of their order of magnitude and to see if the simplification $c_1 = c_{\rho}$ can be introduced. In figure 18(a) we represent the time evolution of the following quantities:

$$\beta_1 = \frac{\|\tau(\rho u_i, u_j)\|_F}{\|\overline{\rho u_i \tilde{u}_j} - \overline{\rho} \tilde{u}_j\|_F}, \quad \beta_{\rho} = \frac{\|\tau(\rho, u_i)\|_F}{\|\overline{\rho u_i} - \overline{\rho} \tilde{u}_i\|_F}, \quad (32)$$

which are analogous to the quantities computed in equations (27) for the eddy viscosity approach. We can notice that both β_1 and β_{ρ} are similar between each other and approximately equal to 1. In order to better quantify the difference between c_1 and c_{ρ} , we represent in figure 18(b) the relative difference between β_1 and β_{ρ} : as we can see



(a)



(b)

Figure 18: (a) Time evolution of the quantities β_1 and β_ρ . (b) Time evolution of the relative difference $|\beta_1 - \beta_\rho|/(\beta_1 + \beta_\rho)/2$ expressed in percentage.

the fact that the two quantities are very similar between each other is confirmed with a relative difference which does not exceed a few percent. It appears, as a consequence, that the simplification $c_1 = c_\rho$ is consistent with the findings of the *a priori* analysis. Notice that, in the similarity scale model case, the simplification $c_1 = c_\rho$ does not lead to the traditional similarity scale model for compressible flows, contrarily to what happens for the eddy viscosity approach where setting $\nu_1 = \nu_\rho$ leads to the traditional model $\bar{\rho}\theta(u_i, u_j) = -\bar{\rho}\nu_1\tilde{\mathcal{S}}_{ij}$

5 Conclusions and future developments

In the present investigation, the theoretical work [12] on LES models for compressible variable density flows has been considered as a starting point for an improved modeling of subgrid scale stresses in compressible flows with respect to the standard approaches.

A first numerical evaluation of the proposed ideas has been provided by means of two-dimensional *a priori* tests. We have found that some terms introduced in [12], which are usually neglected in the common density weighting approach to turbulence models for compressible turbulence, are indeed not negligible. We have also found out that the modeling proposal made in [12] is partially in contrast with the *a priori* tests results themselves.

As a consequence, we have tried to develop alternative proposals for turbulence modelling in variable density compressible flows. The first approach is based on the modelization of the two terms $\tau(\rho, u_i)$ and $\tau(\rho u_i, u_j)$ following the eddy viscosity hypothesis. The *a priori* tests show low values for the correlations between the exact subgrid scale terms and the modeled ones, suggesting that the eddy viscosity approach may not be the better choice. However, as already noticed in [2], such low correlations are rather typical for eddy viscosity models. If, in spite the low correlations values, the eddy viscosity approach is preferred, the *a priori* tests results suggest the introduction of two different, dynamically computed eddy viscosities ν_1 and ν_ρ .

As expected (see [28]), the introduction of a scale similarity model for both $\tau(\rho, u_i)$ and $\tau(\rho u_i, u_j)$ considerably improves the results in terms of correlations. The correlations associated to the proposed similarity scale model are also higher than the correlations associated to the traditional similarity scale approach for compressible flows. Considering the *a priori* tests results, the use of a scale similarity model for the terms $\tau(\rho, u_i)$ and $\tau(\rho u_i, u_j)$, possibly with the simplification $c_1 = c_\rho$, appears to be the best choice. However, a final assessment of these proposals will require testing both the proposed eddy viscosity model and the scale similarity model in a three-dimensional LES.

Acknowledgements

This paper is part of the first author's PhD thesis work at Politecnico di Milano. We are happy to acknowledge the continuous help of M. Restelli and M. Tugnoli with the application of the FEMILARO code. Several comments by F. Denaro and M.V. Salvetti have also

been very useful to improve the presentation of some results. The results of this research have been achieved using the computational resources made available at CINECA (Italy) by the LISA high performance computing project *DECLS: Large Eddy Simulation of Density Currents and Variable Density Flows*, HPL13PJ6YS.

References

- [1] A. Abbà, L. Bonaventura, M. Nini, and M. Restelli. Dynamic models for Large Eddy Simulation of compressible flows with a high order DG method. *Computers & Fluids*, 122:209–222, 2015.
- [2] A. Abbà, C. Cercignani, and L. Valdetaro. Analysis of Subgrid Scale Models. *Computer and Mathematics with Applications*, 46:521–535, 2003.
- [3] J. Bardina, J.H. Ferziger, and W.C. Reynolds. Improved turbulence models based on LES of homogeneous incompressible turbulent flows. Technical Report TF-19, Department of Mechanical Engineering, Stanford, 1983.
- [4] C. Bassi, A. Abbà, L. Bonaventura, and L. Valdetaro. Large Eddy Simulation of gravity currents with a high-order DG method. *Communications in Applied and Industrial Mathematics*, 8:128–148, 2017.
- [5] F. Bassi and S. Rebay. High Order Accurate Discontinuous Finite Element Method for the Numerical Solution of the Compressible Navier-Stokes Equations. *Journal of Computational Physics*, 131:267–279, 1997.
- [6] V. K. Birman, J.E. Martin, and E. Meiburg. The non-Boussinesq Lock-exchange problem. Part 2. High-resolution simulations. *Journal of Fluid Mechanics*, 537:125–144, 2005.
- [7] T. Bonometti, M. Ungarish, and S. Balachandar. A numerical investigation of constant volume non-Boussinesq gravity currents in deep ambient. *Journal of Fluid Mechanics*, 673:574–602, 2011.
- [8] R.E. Britter and J.E. Simpson. Experiments on the dynamics of a gravity current head. *Journal of Fluid Mechanics*, 88:223–240, 1978.
- [9] G. Chavent and B. Cockburn. The local projection $p^0 - p^1$ discontinuous Galerkin finite element method for scalar conservation laws. *Mathematical Modelling and Numerical Analysis*, 23:565–592, 1989.

- [10] B. Cockburn and C.W. Shu. TVB Runge-Kutta local projection discontinuous Galerkin finite element method for conservation laws II: general framework. *Mathematics of Computation*, 186:411–435, 1989.
- [11] G. Constantinescu. LES of lock-exchange compositional gravity currents: a brief review of some recent results. *Environmental Fluid Mechanics*, 14:295–317, 2014.
- [12] M. Germano, A. Abbà, R. Arina, and L. Bonaventura. On the extension of the eddy viscosity model to compressible flows. *Physics of Fluids*, 26, 2014.
- [13] M. Germano, U. Piomelli, P. Moin, and W.H. Cabot. A Dynamic Subgrid-Scale Eddy Viscosity Model. *Physics of Fluids*, 3(7):1760–1765, 1991.
- [14] C. Härtel, E. Meiburg, and F. Necker. Analysis and direct numerical simulation of the flow at a gravity-current head. Part 1. Flow topology and front speed for slip and no-slip boundaries. *Journal of Fluid Mechanics*, 418:189–212, 2000.
- [15] H. Huppert and J.E. Simpson. The slumping of gravity currents. *Journal of Fluid Mechanics*, 99:785–799, 1980.
- [16] J.J. Keller and Y.P. Chyou. On the hydraulic lock-exchange problem. *Journal of Applied Mathematics and Physics (ZAMP)*, 42:874–910, 1991.
- [17] J.B. Klemp, R. Rotunno, and W.C. Skamarock. On the dynamics of a gravity current in a channel. *Journal of Fluid Mechanics*, 331:169–198, 1997.
- [18] S.K. Ooi, G. Constantinescu, and L.J. Weber. 2D Large Eddy Simulation of Lock-exchange gravity current flows at high Grashof numbers. *Journal of Hydraulic Engineering*, 133:1037–1047, 2007.
- [19] T.M. Özgökmen, T. Iliescu, and P.F. Fischer. Large Eddy Simulation of stratified mixing in a three-dimensional Lock-exchange system. *Ocean Modelling*, 26:134–155, 2009.
- [20] T.M. Özgökmen, T. Iliescu, P.F. Fischer, A. Srinivasan, and J. Duan. Large Eddy Simulation of stratified mixing in two-dimensional dam-break problem in a rectangular enclosed domain. *Ocean Modelling*, 16:106–140, 2007.
- [21] P. Sagaut. *Large Eddy Simulation for Compressible Flows*. Springer Verlag, 2009.
- [22] J. Shin, S. Dalziel, and P.F. Linden. Gravity currents produced by lock-exchange. *Journal of Fluid Mechanics*, 521:1–34, 2004.

- [23] J.E. Simpson. *Gravity currents in the environment and in the laboratory*. Cambridge University Press, 1997.
- [24] J. Smagorinsky, S. Manabe, and J. Leith Holloway. Numerical results from a nine-level general circulation model of the atmosphere. *Monthly weather Review*, 93:727–768, 1965.
- [25] C.G. Speziale, G. Erlebacher, T.A. Zang, and M.Y. Hussaini. The subgrid-scale modeling of compressible turbulence. *Physics of Fluids*, 31:940–942, 1988.
- [26] R.J. Spiteri and S.J. Ruuth. A new class of optimal high-order Strong Stability Preserving time discretization methods. *SIAM Journal of Numerical Analysis*, 40:469–491, 2002.
- [27] M. Ungarish. Intrusive gravity currents in stratified ambient, shallow-water theory and numerical results. *Journal of Fluid Mechanics*, 535:287–323, 2005.
- [28] B. Vreman, B. Geurts, and H. Kuerten. A-priori tests of large eddy simulation. *Journal of Engineering Mathematics*, 29:299–327, 1995.
- [29] A. Yoshizawa. Statistical theory for compressible turbulent shear flows, with the application to subgrid modeling. *Physics of Fluids*, 29:2152–2164, 1986.

MOX Technical Reports, last issues

Dipartimento di Matematica
Politecnico di Milano, Via Bonardi 9 - 20133 Milano (Italy)

- 19/2018** Menghini, F.; Dede', L.; Quarteroni, A.
Variational Multiscale LES modeling of blood flow in an idealized left human heart
- 18/2018** Antonietti, P.F.; Bonaldi, F.; Mazzieri, I.
A high-order discontinuous Galerkin approach to the elasto-acoustic problem
- 14/2018** Cuffaro, M.; Miglio, E.; Penati, M.; Viganò, M.
Mantle upwelling driven by asymmetric sea-floor spreading at northern Mid-Atlantic ridge
- 15/2018** Simona, A.; Bonaventura, L.; Pagnat, T.; Dalena, B.
High order time integrators for the simulation of charged particle motion in magnetic quadrupoles
- 16/2018** Calissano, A.; Vantini, S.; Arnaboldi, M.
An elephant in the room: Twitter sampling methodology.
- 17/2018** Agosti, A.; Giverso, C.; Faggiano, E.; Stamm, A.; Ciarletta, P.
A personalized mathematical tool for neuro-oncology: a clinical case study
- 13/2018** Gandelli, E.; Penati, M.; Quaglino, V.; Lomiento, G.; Miglio, E.; Benzoni, G.M.
A novel OpenSees element for single curved surface sliding isolators
- 11/2018** Delpopolo Carciopolo L.; Bonaventura L.; Scotti A.; Formaggia L.
A conservative implicit multirate method for hyperbolic problems
- 12/2018** Dal Santo, N.; Deparis, S.; Manzoni, A.; Quarteroni, A.
Multi space reduced basis preconditioners for large-scale parametrized PDEs
- 09/2018** Menafoglio, A.; Grasso, M.; Secchi, P.; Colosimo, B.M.
Profile Monitoring of Probability Density Functions via Simplicial Functional PCA with application to Image Data